Research Article Vol. 33, No. 9 / 5 May 2025 / Optics Express 18709
Optics EXPRESS

Entanglement, squeezing and non-locality limits in filtered two-mode squeezed mixed states

SOUVIK AGASTI[1,2,*]

[1]IMOMEC division, IMEC, Wetenschapspark 1, B-3590 Diepenbeek, Belgium
[2]Institute for Materials Research (IMO), Hasselt University, Wetenschapspark 1, B-3590 Diepenbeek, Belgium
[*]souvik.agasti@uhasselt.be

Abstract: We investigate the entanglement and non-locality between specific spectral components of continuous variable two-mode squeezed mixed states, identifying their limits. These spectral components are selected from output modes using filters commonly employed in optomechanical systems. Both entanglement and non-locality reach their peak when the filters are identical. However, increasing the degree of input squeezing while applying non-identical filters disrupts both entanglement and non-locality, leading to a bell-shaped pattern. Additionally, we provide precise boundaries for entanglement and non-locality. Furthermore, we also evaluate the squeezing of two-mode hybrid quadrature as a measure of entanglement, thereby demonstrating how it remains analogous to logarithmic negativity. Combined with the filter, the population of two-mode squeezed thermal light influences the angle of a maximally squeezed hybrid quadrature.

1. Introduction

Entanglement is a fundamental aspect of the establishment of quantum mechanics which plays a critical role in understanding the Einstein-Podolsky-Rosen (EPR) measurement paradox [1,2]. It had been the key resource in quantum information processing [3], quantum computation [4], quantum teleportation [5], and quantum meterology including gravitational wave (GW) detector [6]. It quantifies the quantum correlation between continuous-variable states. Gaussian states have mainly been in use for the generation, manipulation, and application of continuous variable entangled states [5,7], and therefore, it remained in the intensive interest of the community.

A profound feature of quantum measurement on hybrid systems is its local realism [1,2], which has extensively been used in the field of quantum information science. The test of quantum non-locality versus local realism still remains a gray area to explore. In this context, Bell's inequality has been considered as a satisfactory condition that all local hidden variables follow [8–10]. Several types of Bell's inequalities have been explored so far to test quantum nonlocality [11,12]. All cases use two-body correlation functions as key elements which have been extracted from the two measurement variables at distant places.

The quantum correlated states are generated by using the correlations between a system and ancilla modes, such as two output ports of a beamsplitter [13], signal and idler generated through spontaneous parametric down-conversion process (PDC) [14] usually by using Kerr non-linear systems [15,16], atomic and cavity modes in cavity quantum electrodynamics [17–19]. The entanglement reveals information about the correlation between two systems, which also ensures that the measurement of an observable on one system collapses overall wavefunction into a definite state. In all two-mode entangled states, squeezing is observed as an inevitable phenomenon. In fact, in the case of systems with two-mode squeezing (TMS), the squeezing variance can be used as the entanglement criteria [18,20]. The squeezing of a quantum state refers to the reduction of fluctuation of a quadrature below the fluctuation of a coherent/vacuum state, which is known as the standard quantum limit (SQL). In the case of TMS, a combination of quadratures can be squeezed, whereas the indevidual modes may not necessarily be squeezed.

#557971 https://doi.org/10.1364/OE.557971
Journal © 2025 Received 28 Jan 2025; revised 16 Mar 2025; accepted 4 Apr 2025; published 21 Apr 2025

Optics EXPRESS

The correlations between the spectral components of PDC-generated single-mode squeezing have been studied and applied before, especially in optomechanical systems [17–19]. However, the quantum correlation between the spectral components of the modes of two-mode squeezed entangled lights has not been studied so far, which is, therefore, the main motivation of this article. Entangled sources are of great interest to the quantum optics community because of their broad range of applications, even in GHz microwave sensing and communication; for example, in the case of microwave quantum illumination [21] and heterodyne quantum sensing [22]. The two-mode squeezed vacuum (TMSV) states generated by the PDC process have shown that their spectral components have non-trivial quantum correlations. The frequency sensitive filters can play a crucial role in such experiments. Besides, the presence of thermal noise and reduction of quantum efficiency are the common phenomenon observed in quantum channels. Therefore, it could be an interest to the community to see how the filters impose limitations on quantum communication and sensing in a noisy environment. Experimentally, conditional states have been generated through quantum correlations of multi-mode twin-beam states [14,23]. Also, an effort was made on time-frequency modes [24] and in general, multimode quantum optics [25], one can see that, even though a general framework to deal with multi mode quantum state is established, they do not deal with filtered TMSV.

In real experimental situations, TMSV faces decoherence due to the presence of a thermal environment. The decoherence and thermalization dynamics of TMSV were studied before by analyzing relative entanglement entropy [26,27]. Also, the dynamical behavior of entanglement during thermalization of TMSV to become a two-mode squeezed thermal (TMST) light is well studied before in [28]. The TMSV is observed to lose its non-local behavior through decoherence under thermal environment [8]. Besides, it was realized before that the region of entanglement remains unchanged even though the detection efficiency drops [28]. Even though the interaction of the thermal environment on the TMSV is well studied, the impact of the filter has never been tested so far which we discuss in this article.

Optical filters are often used to pick up a preferable range of frequency bands from the outputs of quantum systems. In this article, we considered two different types of optical filters, e.g. step and exponential filters. Step filters have already been used before to study the quantum correlation between the modes of optomechanical systems [18,19]. The exponential filters have been used before to analyze the time-dependent physical spectrum of light [29] and also in controlling output entanglement in feedback-controlled optomechanical systems [17].

One can witness the entanglement through homo/heterodyne measurement of two-mode hybrid quadrature variance. Two-mode quadrature squeezing has proven before to be an equivalence of logarithmic negativity which is a popular measure of entanglement [18,20,30]. Besides, homodyne detection techniques to perform the quadrature phase amplitude measurement, provide quantum correlation which is a platform for testing Bell inequality efficiently [9,10]. The analysis enables highlights the loopholes in optical experiments as the violation of Bell's inequality should be taken into care.

Earlier we studied thermalization dynamics of entanglement and non-locality of filtered two-Mode squeezed states for two-mode squeezed thermally decohereted field and thermally decohereted two-mode squeezed vacuum [31]. However, in this article we focus on its steady state behavior rather than thermalization dynamics. Therefore, we pick two-mode squeezed thermal field only and drop the thermal decoherence of TMSV, as it ends up into a thermal state loosing its squeezing. We inspect the impact of optical quantum efficiencies on filtered two mode squeezing. Investigation of steady state behavior of thermalized TMS state has more scope of applicability in experimental point of view, rather than its time dynamics. Beside entanglement, we also study squeezing of maximally optimized quadrature which has also been another indicator of entanglement, as it is a experimentally estimable quantity. While determining that, we show together with the filter, how the the population of TMS thermal light influences the angle of a

Optics EXPRESS

maximally squeezed hybrid quadrature. We also determined mixedness of the state to analyze the discrepancy between entanglement and non-locality.

The article is composed as follows. In Sec. II, we discuss the theory of how the filter manipulates the nature of TMSV. We also discuss the impact of detection efficiency in this section. Afterwards, in Sec. III we considered a TMST light to investigate the impact of thermal population along with filter on entanglement. For experimental realization, we quantify entanglement through the squeezing of hybrid quadrature, where we also see how the temperature controls the squeezed quadrature.

2. Filter on TMSV

2.1. Input TMSV

Entangled TMS is typically generated using non-linear optical crystal (z) through the PDC process. Considering r as the amplitude of the input squeezing and fixing the arbitrary phase to be $\pi/2$, the squeezed Bogliubov modes can be represented as

$$\begin{bmatrix} X_I^{out} \\ Y_I^{out} \\ X_S^{out} \\ Y_S^{out} \end{bmatrix} = \begin{bmatrix} \cosh r & 0 & \sinh r & 0 \\ 0 & \cosh r & 0 & -\sinh r \\ \sinh r & 0 & \cosh r & 0 \\ 0 & -\sinh r & 0 & \cosh r \end{bmatrix} \begin{bmatrix} X_I^z \\ Y_I^z \\ X_S^z \\ Y_S^z \end{bmatrix}, \tag{1}$$

where $X_{I,S}^z(t) = \frac{1}{\sqrt{2}}\left(a_{I,S}^z(t) + a_{I,S}^{z\,\dagger}(t)\right)$ and $Y_{I,S}^z(t) = -i\frac{1}{\sqrt{2}}\left(a_{I,S}^z(t) - a_{I,S}^z(t)^\dagger\right)$ are the amplitude and phase quadratures of the multimode bosonic input modes of the bipartite system idler (I) and signal (S), respectively. Details of the PDC process and the generation of TMSV are shown in Fig. 1(A), where the input beams are directed to the non-linear crystal (z). $a_{I,S}^z(a_{I,S}^{z\,\dagger})$ are the corresponding annihilation (creation) operators, which are related to their spectral components through the Fourier transform: $\tilde{a}_{I,S}^z(\omega) = \sqrt{\frac{1}{2\pi}}\int_{-\infty}^{\infty} e^{i\omega t}a^z(t)\,\mathrm{d}t$ and $\tilde{a}^{z\dagger}_{I,S}(-\omega) = \sqrt{\frac{1}{2\pi}}\int_{-\infty}^{\infty} e^{i\omega t}a^{z\dagger}(t)\,\mathrm{d}t$. Therefore, the frequency spectra of the input quadratures are $\tilde{X}_{I,S}^z(\omega) = \frac{1}{\sqrt{2}}\left(\tilde{a}_{I,S}^z(\omega) + \tilde{a}^{z\dagger}_{I,S}(-\omega)\right)$ and $\tilde{Y}_{I,S}^z(\omega) = -i\frac{1}{\sqrt{2}}\left(\tilde{a}_{I,S}^z(\omega) - \tilde{a}^{z\dagger}_{I,S}(-\omega)\right)$. $X_{I,S}^{out}$ and $Y_{I,S}^{out}$ are the outputs obtained after PDC as TMS state. $a_{I,S}^{out}(a_{I,S}^{out\,\dagger})$ are the corresponding annihilation (creation) operators for the outputs of the systems I and S which are related to their frequency spectra through Fourier transform, similar to the input quadratures: $\tilde{X}_{I,S}^{out}(\omega) = \frac{1}{\sqrt{2}}\left(\tilde{a}_{I,S}^{out}(\omega) + \tilde{a^{out}}^{\dagger}_{I,S}(-\omega)\right)$ and $\tilde{Y}_{I,S}^{out}(\omega) = -i\frac{1}{\sqrt{2}}\left(\tilde{a}_{I,S}^{out}(\omega) - \tilde{a^{out}}^{\dagger}_{I,S}(-\omega)\right)$. Accepting optical losses before the light enters into the filter, we obtain the modified input field, on which the filter applies, as

$$\begin{bmatrix} X_{I,S}^{out} \\ Y_{I,S}^{out} \end{bmatrix}_{actual} = \sqrt{\eta_{I,S}} \begin{bmatrix} X_{I,S}^{out} \\ Y_{I,S}^{out} \end{bmatrix}_{ideal} + \sqrt{1-\eta_{I,S}} \begin{bmatrix} X_{I,S}^{vac} \\ Y_{I,S}^{vac} \end{bmatrix} \tag{2}$$

where $X_{I,S}^{vac}, Y_{I,S}^{vac}$ are the vacuum amplitude and phase noise operators correspond to the systems I and S, respectively, and $\eta_{I,S}$ are their corresponding optical quantum efficiencies.

2.2. Filtered output modes

From the continuous field, one can define and extract many independent optical modes (also, shown in Fig. 1(A)), by selecting different time intervals. Filters on the input select a time interval

Optics EXPRESS

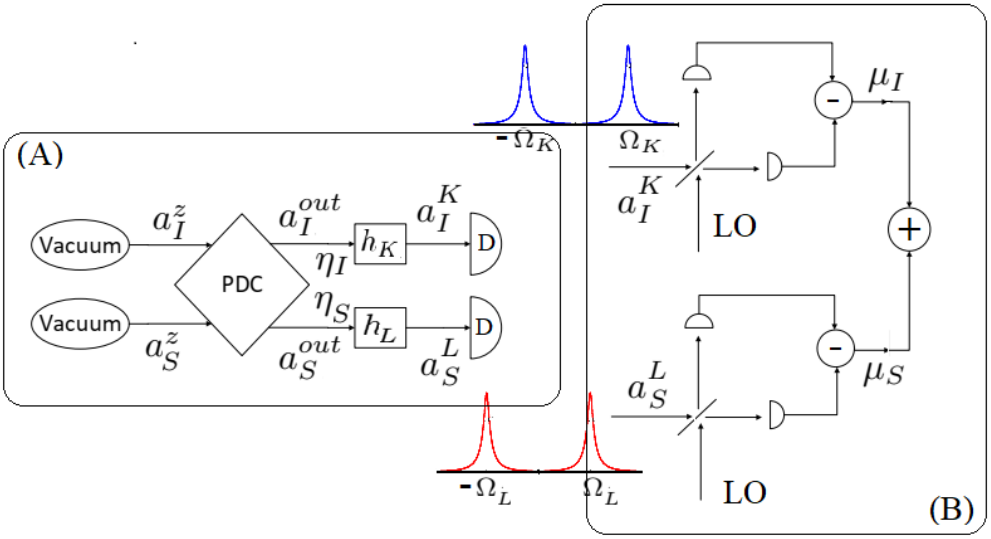

Fig. 1. Block diagram of the detection of filtered TMSV: (A) TMSV is generated using the parametric down-conversion (PDC) process. Optical filters are applied on two-mode squeezed output before being detected at D. (B) Two-mode homodyne detection and the spectral modes are combined with weightage. LO is the local oscillator.

to extract independent output optical modes

$$a_{I,S}^{K,L}(t) = \int_{-\infty}^{t} \mathrm{d}t' h_{K,L}(t-t') a_{I,S}^{out}(t') \tag{3}$$

where $h_{K,L}(t)$ are the filter function of the K, Lth output modes of the bipartite systems I and S, respectively. The regular output field (without filter) follows the correlation function: $[a_k^{out}(t), a_k^{out^\dagger}(t')] = \delta(t-t')$ where $k \in \{I, S\}$. Equivalently, a generic set of output modes, defined in a time interval, obeys the commutation relation: $[a_k^M, a_k^{N^\dagger}] = \delta_{MN}$. This requires to follow the orthonormality between modes, verified by

$$\int_0^\infty h_i(t) h_j^*(t)\, \mathrm{d}t = \delta_{ij} \tag{4}$$

Transforming the filtered output mode, given in Eq. (3) in the frequency domain, one obtains the generalized expression for the field as

$$\tilde{a}_{I,S}^{K,L}(\omega) = \sqrt{2\pi}\tilde{h}_{K,L}(\omega)\, \tilde{a}_{I,S}^{out}(\omega) = \frac{1}{\sqrt{2\pi}} \int_{-\infty}^{\infty} \mathrm{d}t\, a_{I,S}^{K,L}(t)\, e^{i\omega t} \tag{5}$$

where $\tilde{h}_k(\omega)$ are the Fourier transform of the filter function, which also satisfies the orthogonality relation

$$\int_{-\infty}^{\infty} \tilde{h}_i(\omega) \tilde{h}_j^*(\omega)\, \mathrm{d}\omega = \delta_{ij} \tag{6}$$

Here, we choose two different types of explicit sets of filter functions that follow such orthogonality. The type-I is a step filter function, given by

$$h_{K,L}(t) = \frac{\Theta(t) - \Theta(t-\tau_{I,S})}{\sqrt{\tau_{I,S}}} e^{-i\Omega_{K,L}t} \tag{7}$$

where Θ is a Heaviside step function.

Optics EXPRESS

The functions give a set of independent optical modes, distributed around the central frequencies ($\Omega_{K,L}$). $\tau_{I,S}$ are the time duration of corresponding systems I and S. Therefore, $\tau_{I,S}^{-1}$ are the spectral width of the filters which are related to the mode frequencies as

$$\Omega_K - \Omega_{K\pm n} = \pm n\frac{2\pi}{\tau_I} \quad \text{and} \quad \Omega_L - \Omega_{L\pm n} = \pm n\frac{2\pi}{\tau_S}, \quad n \text{ integer} \tag{8}$$

Such filter functions had been in use before in [18,19] for filtering out the output modes of optomechanical systems.

The Fourier transform of the filter function in Eq. (7), can be expressed for different frequency intervals as

$$\tilde{h}_{K,L}(\omega) = \sqrt{\frac{\tau_{I,S}}{2\pi}} e^{i(\omega-\Omega_{K,L})\tau/2} \frac{\sin[(\omega-\Omega_{K,L})\tau_{I,S}/2]}{(\omega-\Omega_{K,L})\tau_{I,S}/2} \tag{9}$$

The central frequencies ($\Omega_{K,L}$) are allowed to vary by an integer multiple of $2\pi/\tau_{I,S}$.

The type-II consists of an exponential filter function, given by

$$h_{K,L}(t) = \frac{e^{-(1/\tau_{I,S}+i\Omega_{K,L})t}}{\sqrt{\tau_{I,S}/2}}\Theta(t), \tag{10}$$

which has frequency spectral distribution in Fourier space

$$\tilde{h}_{K,L}(\omega) = \frac{\sqrt{\tau_{I,S}/\pi}}{1 - i\tau_{I,S}(\omega-\Omega_{K,L})}. \tag{11}$$

The periodicity of this filter function remains the same as Eq. (8). Such exponential filters have been used before in [17,29] to analyze the time-dependent spectrum of light in optomechanical systems.

2.3. Stationary correlation matrix

To determine the correlation matrix, we need to determine the quadratures of the filtered output. For both the step and exponential filters, an infinite number of mutually independent output quadratures can also be defined, by tuning their frequencies and bandwidths. However, in the case of two-mode squeezing, the filtered quadratures can be determined as

$$\begin{bmatrix} X_{I,S}^{K,L}(r;t) \\ Y_{I,S}^{K,L}(-r;t) \end{bmatrix} = \int_{-\infty}^{t} \mathrm{d}t' T_{K,L}(t-t') \begin{bmatrix} X_{I,S}^{out}(r;t') \\ Y_{I,S}^{out}(-r;t') \end{bmatrix} \tag{12}$$

where

$$T_{K,L}(t) = \begin{bmatrix} \Re(h_{K,L}) & -\Im(h_{K,L}) \\ \Im(h_{K,L}) & \Re(h_{K,L}) \end{bmatrix} \tag{13}$$

and the dimensionless amplitude and phase quadrature operators of the outputs of the bipartite systems are defined by $X_{I,S}^{K,L}(r;t) = (a_{I,S}^{K,L}(r;t) + a_{I,S}^{K,L}(r;t)^{\dagger})/\sqrt{2}$, $Y_{I,S}^{K,L}(r;t) = -i(a_{I,S}^{K,L}(r;t) - a_{I,S}^{K,L^{\dagger}}(r;t))/\sqrt{2}$. Following Eq. (12), in the frequency domain, the filtered quadratures can be calculated as

$$\begin{bmatrix} \tilde{X}_{I,S}^{K,L}(r;\omega) \\ \tilde{Y}_{I,S}^{K,L}(-r;\omega) \end{bmatrix} = \sqrt{2\pi}\tilde{T}_{K,L}(\omega) \begin{bmatrix} \tilde{X}_{I,S}^{out}(r;\omega) \\ \tilde{Y}_{I,S}^{out}(-r;\omega) \end{bmatrix} \tag{14}$$

where $\tilde{T}(t)$ is the Fourier transformed matrix of $T_{K,L}(t)$ given in Eq. (13).

Optics EXPRESS

One can obtain the correlation matrix of $V(r)$ at a time t, with the elements

$$V_{ij}(r) = \frac{1}{2}\langle v_i^{out} v_j^{out} + v_j^{out} v_i^{out} \rangle \tag{15}$$

where

$$v^{out} = [X_I^K(r), Y_I^K(r), X_S^L(r), Y_S^L(r)]^T \tag{16}$$

Likewise Eq. (15), by selecting the elements for the squeezing factor $+r$, we obtain the correlation matrix as $V(r) = \begin{bmatrix} V_I & V_{corr}^T \\ V_{corr} & V_S \end{bmatrix}$, where

$$V_I(t) = \begin{bmatrix} V_{11} & V_{12} \\ V_{21} & V_{22} \end{bmatrix} = \frac{1}{2}\mathrm{Diag}[D_I, D_I], \tag{17a}$$

$$V_S(t) = \begin{bmatrix} V_{33} & V_{34} \\ V_{43} & V_{44} \end{bmatrix} = \frac{1}{2}\mathrm{Diag}[D_S, D_S] \text{ and} \tag{17b}$$

$$V_{corr}(t) = \begin{bmatrix} V_{31} & V_{32} \\ V_{41} & V_{42} \end{bmatrix} = \frac{1}{2}\begin{bmatrix} C_{11} & C_{12} \\ C_{21} & C_{22} \end{bmatrix}. \tag{17c}$$

Taking into account optical quantum efficiencies ($\eta_{I,S}$), the elements of the steady state correlation matrix for each mode of the filtered output of the bipartite system are

$$D_I = (1 + 2\eta_I \sinh^2 r), \tag{18a}$$

$$D_S = (1 + 2\eta_S \sinh^2 r), \tag{18b}$$

$$C_{11} = -C_{22} = \sqrt{\eta_I \eta_S} K_f \sinh(2r), \tag{18c}$$

$$C_{12} = C_{21} = 0, \tag{18d}$$

where the element K_f can be determined as

$$K_f = \frac{\sin[\tau(\Omega_K - \Omega_L)]}{\sqrt{\tau_I \tau_S}(\Omega_K - \Omega_L)} \tag{19a}$$

for Type-I step filters: Eq. (7)

$$= \frac{2\sqrt{\tau_I \tau_S}(\tau_I + \tau_S)}{\tau_I^2 \tau_S^2 (\Omega_K - \Omega_L)^2 + (\tau_I + \tau_S)^2} \tag{19b}$$

for Type-II exponential filters: Eq. (10)

where $\tau = \min[\tau_I, \tau_S]$. The value of K_f drops down from its unit value when the filters are not identical, i.e., $\Omega_K \neq \Omega_L$ and $\tau_I \neq \tau_S$, for both the types of filters.

Optics EXPRESS

2.4. Two-mode entanglement and squeezing

The entanglement between two parties can be witnessed by determining the quantity [30]

$$E_N = \max[0, -\ln 2\nu^-], \tag{20}$$

where

$$\nu^- = \sqrt{\frac{\Sigma(V) + \sqrt{\Sigma(V)^2 - 4\det(V)}}{2}} \tag{21}$$

where $\Sigma(V) = (\det V_I + \det V_S - 2\det V_{corr})$

We visualize how the entanglement between the filtered outputs of the bipartite system changes with filter parameters in Fig. 2. Firstly, we vary filter frequencies for both the parties, maintaining linewidth unchanged in Fig. 2(a), and observe the entanglement to be maximized when the central frequencies match ($\Omega_K = \Omega_L$) for both the types of filters. It also shows a drastic drop in the entanglement when the central frequencies mismatch ($\Omega_K \neq \Omega_L$). This happens due to disruption of coherent transfer of the output light through the filter. Similarly, the entanglement also shows to be maximized when the bandwidth matches ($\tau_I = \tau_S$) in Fig. 2(b) and drops down with mismatch, which is also caused by the imbalanced transfer of output state through the filter. Anticipating that, however, interestingly we see, unlike central frequencies, the region of entanglement becomes wider with the increment of time duration ($\tau_{I,S}$), i.e., the decrement of spectral width. The phenomenon can easily be justified from the fact that, in the case of the larger ($\tau_{I,S}$), the linewidth of the filter becomes narrower, which therefore ensures a smaller probability of frequency mismatch and the greater the entanglement. Besides, we observe a difference between type-I and type-II filters, i.e., compared to the type-I filter, the region of entanglement becomes narrower for the variation of central frequencies and wider for the variation of bandwidths for the type-II filter. The impact of filter frequencies and their bandwidths can simply be taken into account with the factor K_f given in Eq. (19).

The mismatch of frequencies and bandwidths eventually decreases K_f given in Eq. (19). Figure 3(I) shows how the entanglement increases initially and decreases further with the increment of input degree of squeezing (r), making a bell shape. The entanglement shows to have an upper cutoff limit for the input degree of squeezing squeezing $\left(E_N(r \geq r_{ucf}^{EN}) = 0\right)$, which is determined by K_f as

$$\tanh(r_{ucf}^{EN}) = K_f. \tag{22}$$

Figure 3(a,I) shows the bell shape becomes narrower and the entanglement is also observed to destroy with the decrement of K_f from its unit value. Therefore, the upper cutoff shrinks with the mismatch of filter parameters. It remains unchanged irrespective of optical quantum efficiencies ($\eta_{I,S}$), even though the entanglement between the filtered output modes has shown to have a significant dependency on them (Fig. 3(b,I)). Earlier, it was realized that the entangled state always remains entangled irrespective of detection efficiency [28]. The phenomenon remains unchanged even after applying filer on output, as the entanglement is seen to be robust against the decrement of detection quantum efficiency. However, the entanglement was reduced with the reduction of detection efficiency, also shown in Fig. 3(b,I). The entanglement reaches its' maximum for the input squeezing r_{max}^{EN}, where

$$\tanh(2r_{max}^{EN}) = \left(\frac{\sqrt{4\eta_I\eta_S K_f^2 \left(2\eta_I\eta_S + (\eta_S + \eta_I)\sqrt{\left(1 - K_f^2\right)\eta_I\eta_S} - \eta_I\eta_S K_f^2\right)}}{\left(2\eta_I\eta_S + (\eta_S + \eta_I)\sqrt{\left(1 - K_f^2\right)\eta_I\eta_S}\right)} \right). \tag{23}$$

Optics EXPRESS

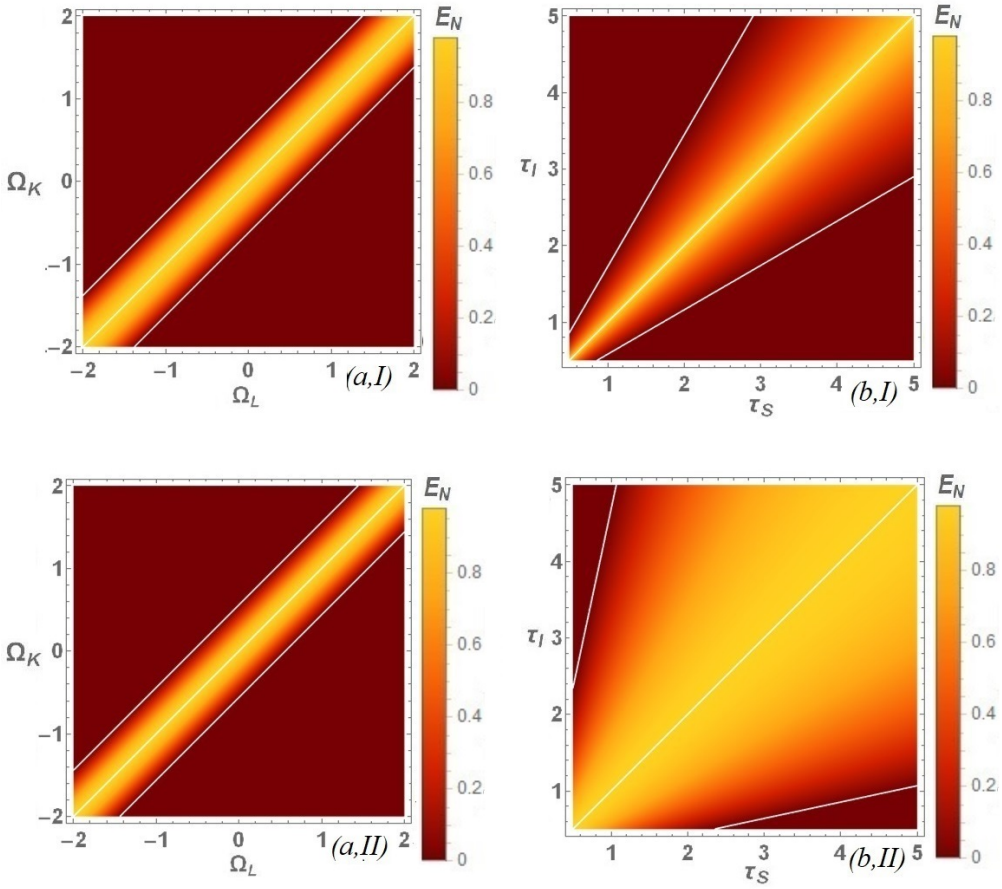

Fig. 2. Entanglement between filtered outputs for the variation of parameters of (a) central frequencies for $\tau_I = \tau_S = 2\Omega_K^{-1}$) (b) filter linewidths for $\Omega_L = \Omega_K$), for (I)step filter and (II) exponential filter. Fixed parameter is $r = 1$. White lines indecate the boundary and maxima of entanglement.

r_{max}^{EN} can be maximized when the condition $\eta_I = \eta_S$ satisfies. In that situation, the entanglement profile becomes uniformly bell-shaped and the maximum is obtained at $r_{max}^{EN} = \frac{1}{2} r_{ucf}^{EN}$.

Since, we start with a TMSV and entanglement encourages to investigate the two-mode squeezing between two party filtered quadratures. The filtered arbitary composite quadrature operator (angle ϕ_I and ϕ_S, respectively) of the two-party system for the output is

$$X_{IS}^{KL(\phi_I\phi_S)} = \frac{1}{\sqrt{2}}(e^{-i\phi_I} a_I^K + e^{i\phi_I} a_I^{K\dagger} + e^{-i\phi_S} a_S^L + e^{i\phi_S} a_S^{L\dagger}). \tag{24}$$

We evaluate the fluctuation of the two-party filtered quadrature operator:

$$S_q(X_{IS}^{KL(\phi_I\phi_S)}) = \frac{1}{2}\langle\{X_{IS}^{KL(\phi_I\phi_S)}, X_{IS}^{KL(\phi_I\phi_S)}\}\rangle \tag{25}$$

The maximally squeezed quadrature is realized for $\phi_I + \phi_S = \pi$. The squeezing becomes maximum for the value of r:

$$\tanh(2r_{max}^{SQ}) = \frac{2\sqrt{\eta_I\eta_S}K_f}{\eta_I + \eta_S}. \tag{26}$$

Optics EXPRESS

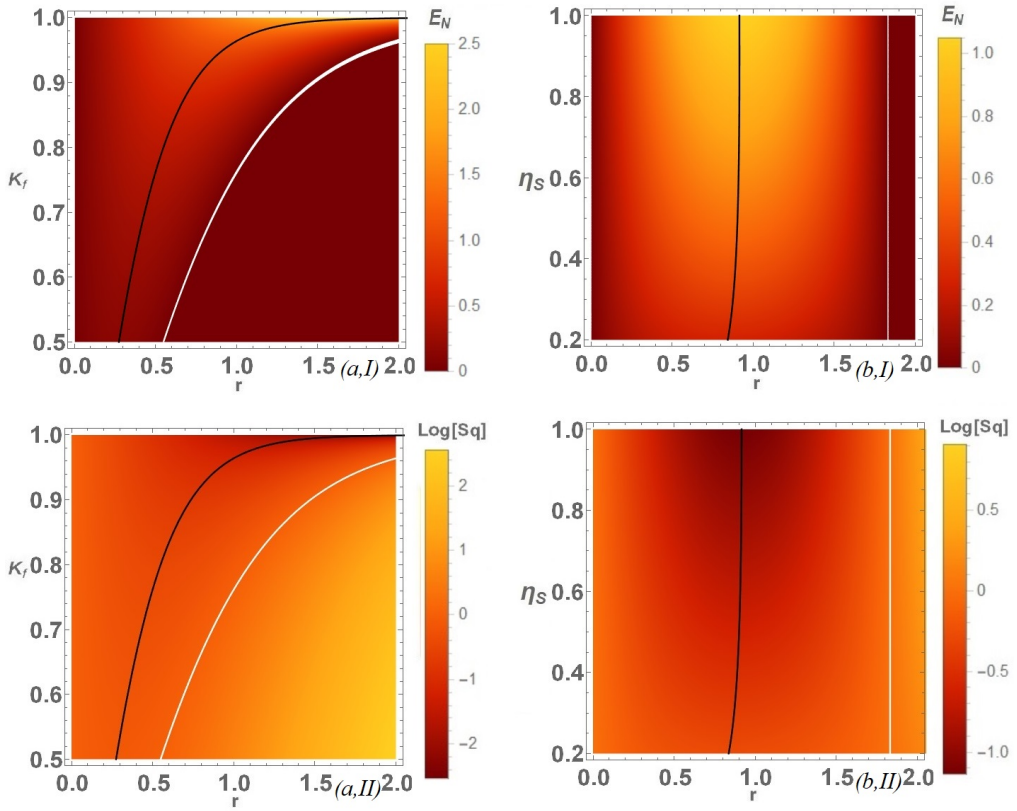

Fig. 3. Entanglement (I) and maximally optimized squeezing (II) between filtered outputs for the variation of parameters: (a) K_f and r for fixed optical quantum efficiencies $\eta_I = 0.9, \eta_S = 0.98$, and (b) η_S and r for fixed $K_f = 0.95$ and $\eta_I = 0.9$. Black lines stand for the maximal entanglement and squeezing, and white lines indecate the boundary of entanglement and SQL.

The squeezing of the hybrid quadrature disappears as the fluctuation (S_q) rises above the SQL, when the input squeezing increases to $r_{ucf}^{SQ} = 2r_{max}^{SQ}$. Note that the cutoff limit of squeezing (r_{ucf}^{SQ}) is dependent on optical quantum efficiencies, and therefore different than r_{ucf}^{EN}. Both limits match together only when the quantum efficiencies match ($\eta_I = \eta_S$).

Squeezing and entanglement are two very related concepts, as we know that the squeezing variance can be used as entanglement criteria [18,20]. The squeezing variance is estimated for the hybrid quadratures constructed with a weighted mixture of the output photocurrent as shown in Fig. 1(B). The weighted quadrature is

$$X_{IS(\mu_I\mu_S)}^{KL(\phi_I\phi_S)} = \frac{1}{\sqrt{\mu_I^2+\mu_S^2}}\left[\mu_I e^{i\phi_I}a_I^K + \mu_I e^{-i\phi_I}a_I^{K^\dagger} + \mu_S e^{i\phi_S}a_S^L + \mu_S e^{-i\phi_S}a_S^{L^\dagger}\right] \tag{27}$$

where μ_I, μ_S are the weight parameters introduced as the scaling of two systems, considered to be real and positive.

Adapting the balance between weights, we obtain maximal squeezing (see Appendix A)

$$S_q(X_{IS}^{KL})_{optimized} = 1 + (\eta_I + \eta_S)\sinh^2(r) - \sinh(r)\sqrt{4\eta_I\eta_S K_f^2\cosh^2(r) + (\eta_I - \eta_S)^2\sinh^2(r)} \tag{28}$$

Optics EXPRESS

The maximally optimized squeezing of the two-mode hybrid quadrature shows a behavior similar to entanglement, which can be visualized in Fig. 3(II). The plots also show the boundary where the squeezing goes beyond SQL, lies the same with the entanglement limits as it is seen in Fig. 3(I). The optimized two-mode squeezing is observed to be maximized at $r = r_{max}^{EN}$. One can obtain two modes squeezing below SQL till $r \leq r_{ucf}^{EN}$; outside which, the fluctuation can not be suppressed below SQL. At this limit the weight ratio becomes $\frac{\mu_I}{\mu_S} = \sqrt{\frac{\eta_S}{\eta_I}}$.

2.5. Purity of state

The entanglement becomes necessary and sufficient criteria of non-locality for pure states. However, in the case of mixed states, it is not true, and therefore, it is essential to investigate the purity of the states. The purity of states are determined from their density matrix [32]. The Gaussian states are characterized by their Wigner function, which is expressed by

$$W(u_M) = \frac{1}{\pi^2\sqrt{\det[V(r)]}} \exp\left[-\frac{1}{2}u_M{}^T V(r)^{-1} u_M\right], \tag{29}$$

where $u_M = [Q_I, P_I, Q_S, P_S]^T$ is the common vector of the fluctuation of two modes. The purity of the state (ρ) is measured by

$$\mathrm{Tr}[\rho^2] = \frac{\pi^2}{4}\int_R W^2(u_m)\mathrm{d}u_m \tag{30}$$

which gives

$$\mathrm{Tr}[\rho^2] = \frac{1}{|C_{11}^2 + C_{12}^2 - D_I D_S|} \tag{31}$$

which is unit valued for vacuum and TMSV, clearly indicating pure states. However, non-identical filters on output destroy the purity, observed in Fig. 4(a). The mixness of the state is also observed to increase with the decrement of detection quantum efficiency (Fig. 4(b)). Unlike entanglement, in both cases, the purity is always observed to reduce with the increment of input squeezing (r).

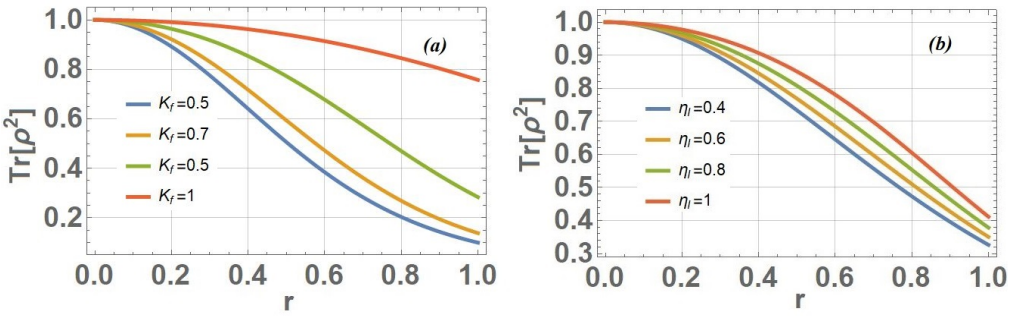

Fig. 4. Purity of the TMSV as a function of r, for (a) fixed optical quantum efficiencies $\eta_I = 0.9, \eta_S = 0.98$, and (b) fixed $K_f = 0.95$ and $\eta_I = 0.9$.

2.6. Quantum non-locality

Quantum nonlocality of two-party entangled continuous variables is a natural interest of measurement. A given state is considered to be non-local when it violates Bell's inequality. The

Optics EXPRESS

Bell's inequality is defined to be $|B|_{max} \leq 2$ using maximum value of the Bell's function (B), which can be expressed in terms of Wigner functions as [8,33]

$$B = \frac{\pi^2}{4}\left[W(u_M^{00}) + W(u_M^{01})W(u_M^{10}) - W(u_M^{11})\right] \tag{32}$$

where $u_M^{mn} = [Q_I^m, P_I^m, Q_S^n, P_S^n]^T$. Such type of Bell's inequality was first described by Clauser, Horne, Shimony and Holt [11]. In quantum mechanics, joint probability distributions are often been expressed using the Q-function or Wigner function. Therefore, the Wigner function has always remained to be useful to test quantum non-locality. Even though violation of all possible Bell's inequalities are not necessary criteria of being nonlocal; in the case of TMS states, violation of Bell's inequality confirms non-locality [33,34].

Quantum mechanically, the field is considered to be nonlocal when $|B|_{max}$ reaches above 2 and the non-locality gets stronger as $|B|_{max}$ becomes larger. We determine $|B|_{max}$ numerically for the non-identical filters in Fig. 5. Likewise entanglement or squeezing profile, we observe the Bell function to drop down with the initial degree of squeezing (r). Also, the region of nonlocality reduces rapidly with the reduction of K_f from its unit value (Fig. 5(a)). However, unlike entanglement, even in the case of identical filters, the region of non-locality is limited concerning the initial degree of squeezing. Besides, we also realize from Fig. 5(b) that the region of non-locality reduces with the reduction of output quantum efficiency, which is a distinct difference compared to the entanglement profile in Fig. 3(b). Overall, the region of quantum non-locality appears to lie within the territory of entanglement, which can be justified by the mixedness of states.

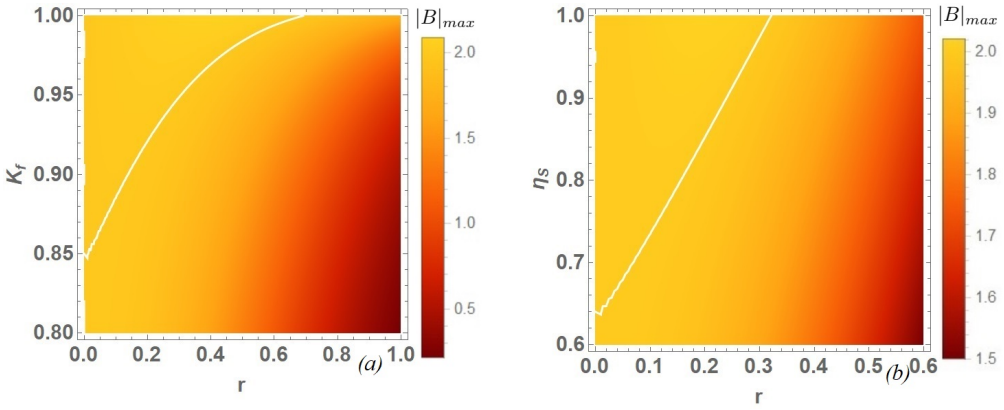

Fig. 5. The maximal value of Bell function as a function of (a) K_f and r for $\eta_I = 0.9, \eta_S = 0.98$, and (b) η_S and r by fixing $\eta_I = 0.9, K_f = 0.95$. White lines indecate the boundary of non-locality.

For pure states the violation of Bell inequalities occurs if and only if the state is entangled. However, for mixed states, entanglement is necessary but not sufficient to ensure the violation of Bell inequality [35] . The investigation of purity of the state appears in this context while studying the violation of Bell's inequality to compare with entanglement limits.

3. Two mode squeezed thermal state

3.1. Entanglement and squeezing

We furthermore considered TMST light to study the impact of filters on it. The basic block diagram is given in Fig. 6. Such states, even though have already been studied before in [27,28],

Optics EXPRESS

the impact of filter on squeezed output have not been investigated. Adding up filters given in Eqs. (7), (10) into the model of squeezed thermal states, gives us interesting features to be studied. The effective thermal population of the multimode input light is controlled by the temperature and the frequencies that we are interested in. Previously, we have analyzed the dynamical evolution of the filtered TMS state throughout thermalization in [31]. Therefore, in this article we focus on steady state behavior only to find its' limits of entanglement, squeezing and non-locality. The elements of the correlation matrix of the Eq. (17) gives

$$D_I = B + A\cosh(2r) \tag{33a}$$

$$D_S = -B + A\cosh(2r) \tag{33b}$$

$$C_{11} = -C_{22} = AK_f \sinh(2r) \tag{33c}$$

$$C_{12} = C_{21} = -BL_f \sinh(2r), \tag{33d}$$

where the elements A, B and L_f are given by

$$A = n_I + n_S + 1,\ B = n_I - n_S, \tag{34a}$$

$$\begin{aligned} L_f =& \frac{1-\cos\left(\tau\left(\Omega_K-\Omega_L\right)\right)}{\sqrt{\tau_I\tau_S}\left(\Omega_K-\Omega_L\right)} \text{for Type-I step filters: Eq. (7)} \\ =& \frac{2(\tau_I\tau_S)^{3/2}(\Omega_K-\Omega_L)}{\tau_I^2\tau_S^2(\Omega_K-\Omega_L)^2+(\tau_I+\tau_S)^2} \\ & \text{for Type-II exponential filters: Eq. (10)} \end{aligned} \tag{34b}$$

where $\tau = \min[\tau_I, \tau_S]$ and κ_I and κ_S are the rates of dissipation, n_I, and n_S are the thermal quanta of their corresponding reservoir for the systems I and S, respectively. Since the entanglement limits have not been changed due to optical efficiencies, we have chosen the detection efficiency to be fixed and maximized for this section of the article. One can always determine the steady state correlation matrix and find the Eq. (17) for a situation when the reservoir is a vacuum.

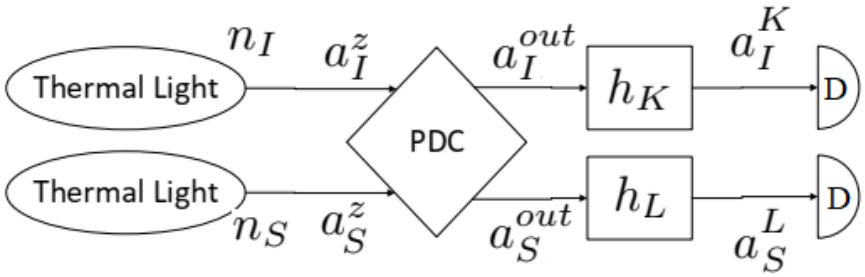

Fig. 6. Block diagram of the generation and detection of filtered TMS thermal light. The only difference with Fig. 1 is the input source is replaced by a thermal light.

In the case of thermally populated reservoirs, the entanglement at steady state shows to have both upper and lower cutoff limits for the input squeezing parameters ($r_{ucf}^{EN} \geq r \geq r_{lcf}^{EN}$),

Optics EXPRESS

representing separability condition. Both the upper and lower limits are determined as

$$\cosh(2r_{ucf}^{EN}) = \frac{A + \sqrt{\left(A^2\left(K_f^2-1\right)+B^2L_f^2\right)\left(A^2K_f^2+B^2\left(L_f^2-1\right)+1\right)+A^2}}{A^2\left(1-K_f^2\right)-B^2L_f^2} \tag{35a}$$

$$\cosh(2r_{lcf}^{EN}) = \frac{A - \sqrt{\left(A^2\left(K_f^2-1\right)+B^2L_f^2\right)\left(A^2K_f^2+B^2\left(L_f^2-1\right)+1\right)+A^2}}{A^2\left(1-K_f^2\right)-B^2L_f^2} \tag{35b}$$

The steady-state entanglement between two filtered modes has been plotted in Fig. 7 for (a) identical filters ($\Omega_K = \Omega_L$) and ($\tau_I = \tau_S$), and therefore $K_f = 1$ and $L_f = 0$, and for (b,I) non-identical filters: $\Omega_K \neq \Omega_L$ and $\tau_I \neq \tau_S$ resulting K_f<1 and L_f>0. As witnessed from the Eq. (35), the upper limit of squeezing factor (r_{ucf}^{EN}) blows up for the perfect homodyne detection when the filters are identical. However, one can anticipate a lower limit of the input degree of squeezing even in case of identical filters or no filters applied on outputs (Fig. 7(a)). The entanglement declines with the increment of thermal populations of the reservoirs. This moreover ensures an extension of the lower cutoff (r_{lcf}^{EN}) in both the cases Fig. 7(a) and (b). Besides, the upper cutoff (r_{ucf}^{EN}) is observed to shrink down with thermal populations in case of non-identical filters in Fig. 7(b) which can be anticipated from Eq. (35). The entanglement is maximized for the input squeezing parameter (r_{max}^{EN}) when

$$\cosh(2r_{max}^{EN}) = \frac{\sqrt{A^2B^2\left(L_f^2-1\right)+A^4K_f^2}}{\sqrt{\left(A^2K_f^2+B^2L_f^2\right)\left(A^2\left(1-K_f^2\right)-B^2L_f^2\right)}} \tag{36}$$

While estimating two-mode squeezing, the maximally squeezed quadrature is realized for $\phi_I + \phi_S = \pi - \zeta$, where $\zeta = \arctan(\frac{BL_f}{AK_f})$. One can notice that the squeezing angle shifts with the change in the thermal population of the initial thermal light and the filter parameters. The thermal population can be dependent on the temperature and the frequency of interest. The angle of the filtered quadratue remains unchanged to the initial squeezing angle (i.e. $\zeta = 0$) only when the thermal population of both the reservoirs matches ($n_1 = n_2$) or two filters are identical ($L_f = 0$). The angle of the maximally squeezed quadrature is plotted in Fig. 7(c) where the squeezed quadrature exhibits a clear dependence on thermal population.

The squeezing of the filtered arbitrary composite quadrature $S_q(X_{IS}^{KL(\phi_I\phi_S)})$ given in Eq. (24) shows to have boundaries of the lower (r_{lcf}^{SQ}) and upper (r_{ucf}^{SQ}) cutoff limits within which the squeezing goes below SQL, where

$$\tanh(r_{lcf}^{SQ}) = \frac{\sqrt{A^2K_f^2+B^2L_f^2}-\sqrt{A^2K_f^2-A^2+B^2L_f^2+1}}{A+1} \tag{37a}$$

$$\tanh(r_{ucf}^{SQ}) = \frac{\sqrt{A^2K_f^2+B^2L_f^2}+\sqrt{A^2K_f^2-A^2+B^2L_f^2+1}}{A+1}. \tag{37b}$$

The squeezing hits the standard quantum limit. The squeezing reaches to its maximum for r_{max}^{SQ}, where

$$\tanh(2r_{max}^{SQ}) = \frac{1}{A}\sqrt{A^2K_f^2+B^2L_f^2} \tag{38}$$

Optics EXPRESS

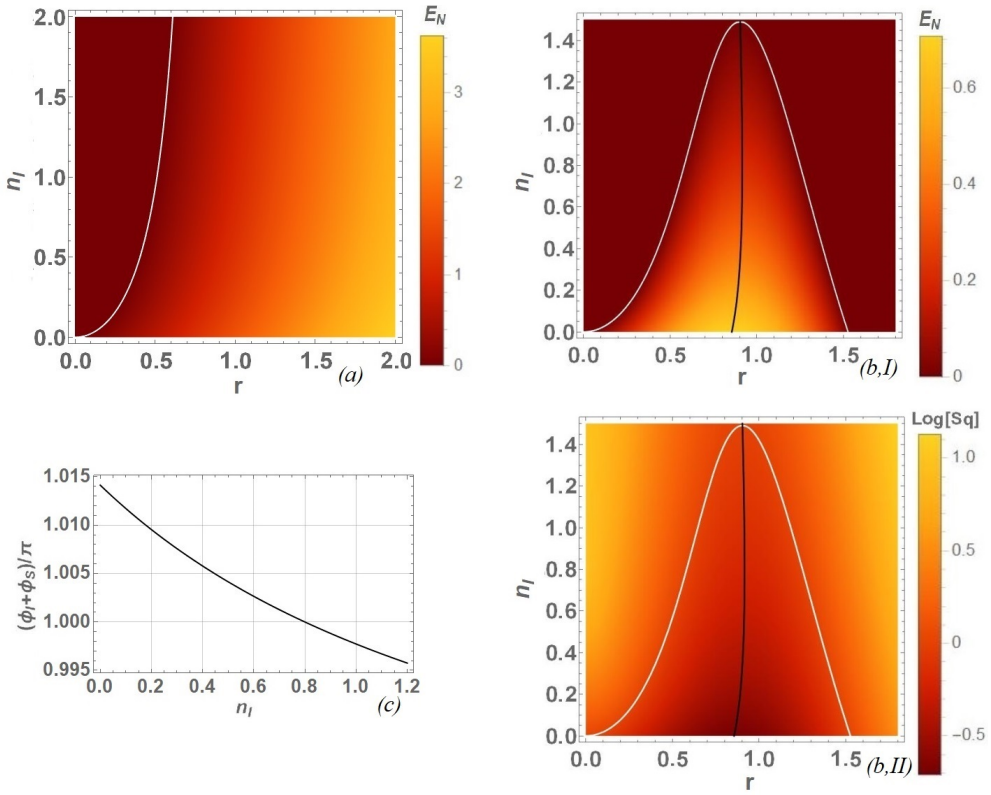

Fig. 7. Entanglement of the filtered outputs for (a) identical filters: $K_f = 1, L_f = 0$ which shows the lower entanglement boundary of (r). Entanglement (b,I), maximally optimized squeezing (b,II) and Maximally squeezed hybrid quadrature as a function of thermal population n_I (c) for non-identical filters $K_f = 0.95, L_f = 0.095$ which gives both the lower and upper limits of entanglement. Black lines stand for the maximal entanglement and squeezing, and white lines indecate the boundary of entanglement and SQL. For all the cases $n_S = 0.8$ and the optical quantum efficiencies $(\eta_{I,S})$ are considered to be 1.

In case of weighted quadratures $(X^{KL(\phi_I\phi_S)}_{IS(\mu_I\mu_S)})$ defined in Eq. (27), accepting the optimized weight (see Appendix A), the maximally squeezed quadrature becomes

$$S_q(X^{KL}_{IS})_{optimized} = A\cosh(2r) - \sqrt{\sinh^2(2r)\left(A^2K^2 + B^2L^2\right) + B^2} \tag{39}$$

The lower and upper cutoff boundaries of the input squeezing are obtained to be (r^{EN}_{lcf}) and (r^{EN}_{ucf}) determined in Eq. (35), for the maximally optimized squeezed quadratures within which the squeezing goes beyond SQL. The lower and upper cutoff borders are exhibited in Fig. 7(b,II), where we see the region of squeezing follows exactly same to the region of entanglement in Fig. 7(b,I), and therefore, reduces with the increment of thermal population. Also, one can obtain maximum squeezing for the value of input squeezing r^{EN}_{max} given in Eq. (36).

3.2. Purity of the state

As we discussed before, in case of pure states, entanglement ensures non-locality, which is not true for a mixed state. For mixed states, entanglement is necessary but not sufficient for non-locality, which therefore, motivates to determine the purity of the TMST state. We estimate

Optics EXPRESS

the purity of the TMST light in Fig. 8 and notice that the purity of the state goes down with an increasing thermal population. However, the purity remains unchanged with increasing input squeezing for identical filters. Furthermore, it is also observed that the purity is destroyed with increasing input squeezing when the filters are non-identical.

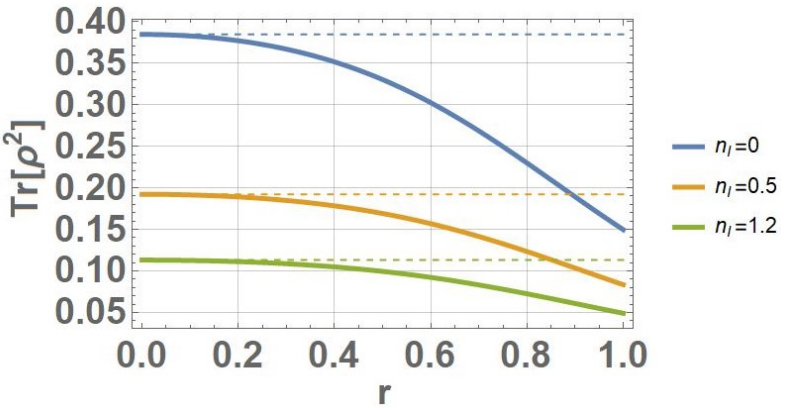

Fig. 8. Purity of the TMS thermal state as a function of r are represented by thick solid lines for fixed $K_f = 0.95$, $L_f = 0.095$ and $n_S = 0.8$. Thin dashed lines represent purity of that state without/idetical filters ($K_f = 1, L_f = 0$). All optical quantum efficiencies are fixed to 1.

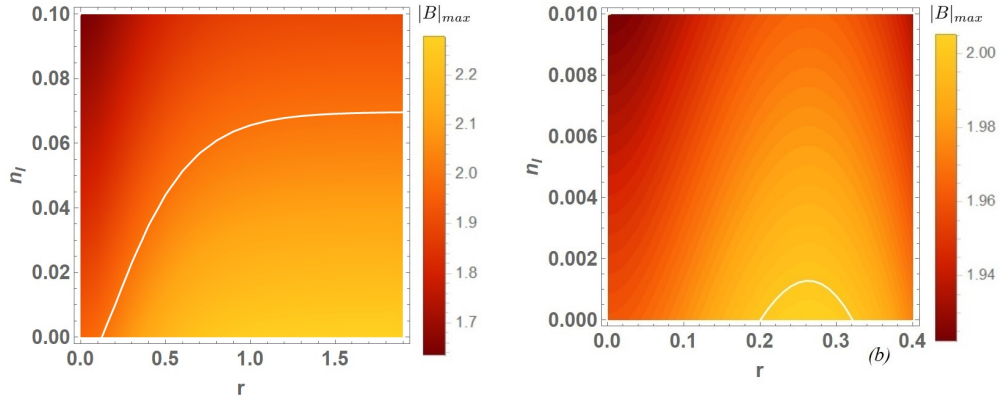

Fig. 9. The maximal value of Bell function as a function of n_I and r for idential filters in (a), and (b) non-identical filters: $K_f = 0.95$, $L_f = 0.095$. Both the cases $n_S = 0.01$. The optical quantum efficiencies ($\eta_{I,S}$) are always considered to be 1. White lines indecate the boundary of non-locality.

3.3. Quantum non-locality

We determine the region of quantum non-locality for the TMS thermal state in Fig. 9. Following entanglement limits, in the case of identical filters, Fig. 9(a) only exhibits a lower boundary of non-locality. Anticipating that, however, unlike Fig. 7(a), the boundary of nonlocality in Fig. 9(a) seems to reach a plato of the input thermal population, while increasing initial degree of squeezing (r). Besides, following entanglement limits in Fig. 7(b), the non-locality seems to show an upper limit for non-identical filters in Fig. 9(b), leaving a tiny region for non-local measurements. Moreover, the observation concludes that the region of quantum non-locality

Optics EXPRESS

ensures entanglement, but the entanglement does not ensure non-locality, which can be justified from the mixness of the state. Rapid destruction of non-locality due to the influence of thermal bath was witnessed before in [8], however, the impact of filter has not been discussed, which is primarily covered here.

4. Conclusion

We investigated the impacts of filters on TMS (Two-Mode Squeezed) states in noisy environment. We found that entanglement is maximized when the filters are identical. The coherent transfer of TMS state through filters only happens when the filtering process is perfectly balanced. For non-identical filters, entanglement decreases with increased input squeezing, creating a bell-shaped curve. We identified the conditions under which entanglement is maximized and determined the cutoff limits. Our findings show that the region of entanglement remains unchanged with variations in detection efficiency, even after applying filters.

In our study of TMST (Two-Mode Squeezed Thermal) light, we observed that entanglement is robust against thermal population. As a complementary measure to logarithmic negativity, we determined the TMS of optimized quadratures, which can be experimentally measured through homodyne or heterodyne detection. The SQL (Standard Quantum Limit) boundaries and maximal squeezing follow the entanglement profile, serving as direct measurements of corresponding logarithmic negativity [18]. The temperature of thermal light, along with the non-identicality of filters, affects the angle of maximally squeezed quadrature. Non-identical filters ensure that the state is mixed. Following the entanglement profile, we also realized that filters limit the non-local measurement of the filtered output. However, unlike entanglement, the region of non-locality decreases with reduced detection efficiency [8–10]. Importantly, because the states are mixed, Bell inequality is violated only if the state is entangled. Therefore, while entanglement has proven to be necessary, it is not sufficient for non-locality.

Optical filters have been used before in optomechanical systems to pick up spectral components [17–19]. Therefore, our analysis of filtered TMS states could be useful in the execution of experiments on hybrid optomechanical systems, which could be used, for example, in GW metrology [6]. Also, uses of two-mode entangled quantum states and the practice of heterodyne detections are quite common even in microwave quantum communication and sensing [21,22]. Besides, we often experience the presence of thermal noise and the reduction of quantum efficiency in quantum channels. The interaction of the thermal environment with TMSV has already been studied before [8,26–28]. Therefore, it is necessary to take into account the filters that impose limitations in noisy quantum channels. Unlike the thermalization dynamics of the filtered TMS states studied previously in [31], we study its steady-state behavior here, which is of more experimental importance. In general, quantum-correlated conditional states have shown immense potential in quantum information and communication [3–5]. Moreover, the destruction of entanglement and non-locality at higher degrees of input squeezing leads us to conclude that generating a highly squeezed two-mode state may not always be beneficial for multimode quantum optical experiments [24,25].

A. Optimization of maximally squeezd quadrature

We estimated the parameter space here where the fluctuation of hybrid quadrature can reach beyond SQL. The fluctuation of a maximally squeezed weighted quadrature is

$$S_q(X^{KL}_{IS(\mu_I\mu_S)}) = \frac{1}{\mu_I^2+\mu_S^2}\left[\mu_I^2 D_I + \mu_S^2 D_S - 2\mu_I\mu_S\sqrt{C_{11}^2 + C_{21}^2}\right] \tag{40}$$

Optics EXPRESS

The optimized weight ratio for which the squeezing is maximum

$$\frac{\mu_I}{\mu_S} = \frac{D_S - D_I + \sqrt{4C_{11}^2 + 4C_{12}^2 + D_I^2 - 2D_I D_S + D_S^2}}{2\sqrt{C_{11}^2 + C_{12}^2}} \tag{41}$$

The generalized phase matching relation for the maximally squeezed quadrature does not change as it was in the case of the TMS thermal state ($\phi_I + \phi_S = \pi - \zeta$, where $\zeta = \arctan(\frac{BL_f}{AK_f})$). Accepting the optimized weight ratio, the maximal TMS quadrature gives

$$S_q(X^{KL}_{IS(\mu_I\mu_S)})|_{optimized} = \frac{1}{2}(D_I + D_S - \sqrt{4C_{11}^2 + 4C_{12}^2 + (D_I - D_S)^2}) \tag{42}$$

A.1. Maximally squeezd TMSV quadrature

The minimized fluctuation of the hybrid quadrature $S_q(X^{KL(\phi_I\phi_S)}_{IS(\mu_I\mu_S)})$ at $\phi_I + \phi_S = \pi$ can further be optimized for the ratio of weights

$$\frac{\mu_I}{\mu_S} = \frac{\sqrt{4\eta_I\eta_S K_f{}^2 + (\eta_I - \eta_S)^2 \tanh^2(r)} + (\eta_S - \eta_I)\tanh(r)}{2K_f\sqrt{\eta_I\eta_S}}. \tag{43}$$

Figure 10(a) shows how the squeezing of maximum squeezed quadrature varies with the change of K_f and the ratio μ_I/μ_S. Based on that, we optimized maximal squeezing (which is plotted by black lines) which remains to be μ_I/μ_S>1 for η_S>η_I. The weight ratio reduces approaching to be unit valued when K_f increases to 1. We also determined how the squeezing varies with the change of r and the ratio μ_I/μ_S in Fig. 10(b), and realized an opposite phenomenon, that the weight ratio for the maximally optimized squeezing increases from its unit value when r increases. We also estimated the borderline where the squeezing goes beyond the SQL for both the cases .

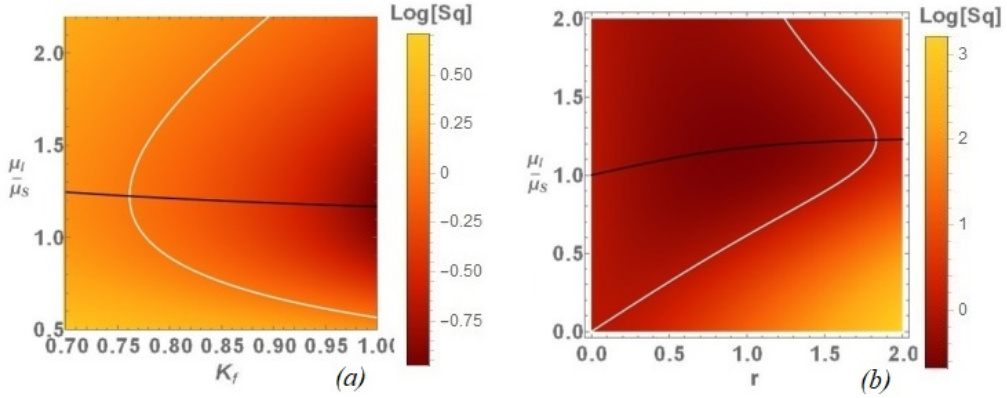

Fig. 10. Squeezing of two parties filtered output for the variation of (a) the weight ratio μ_I/μ_S vs K_f when $r = 1$ and (b) μ_I/μ_S vs r when $K_f = 0.95$. The fixed optical quantum efficiencies $\eta_I = 0.6, \eta_S = 0.9$. Black lines stand for the maximal of squeezing, and white lines indecate the boundary of SQL.

Optics EXPRESS

A.2. Maximally squeezd TMS thermal quadrature

In case of weighted quadratures ($X^{KL(\phi_I\phi_S)}_{IS(\mu_I\mu_S)}$) defined in Eq. (27), the squeezing $S_q(X^{KL(\phi_I\phi_S)}_{IS(\mu_I\mu_S)})$ is maximized for the weight ratio

$$\frac{\mu_I}{\mu_S} = \frac{\sqrt{\sinh^2(2r)\left(A^2K_f^2 + B^2L_f^2\right) + B^2} - B}{\sinh(2r)\sqrt{A^2K_f^2 + B^2L_f^2}} \tag{44}$$

We visualize how the combined quadrature variance changes with the variation of the thermal population in Fig. 11(b-I) and input squeezing factor in Fig. 11(b-II). The ratio reduces with the increment of the thermal population (n_I) and the weights become equal when the population matches ($n_I = n_S$). Furthermore, we also realize the weights approach towards equality with the increment of input squeezing, which can also be hinted from the Eq. (44). In both cases, we also determined the boundaries beyond which the squeezing below SQL disappears.

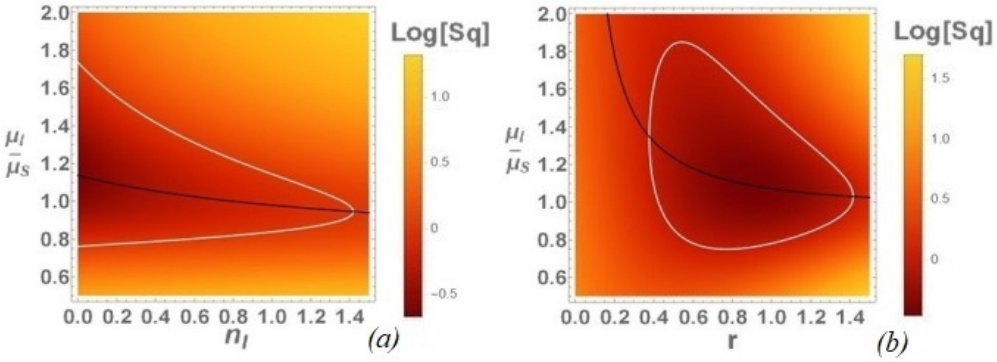

Fig. 11. Squeezing of two parties filtered output for the variation of (a) the weight ratio μ_I/μ_S vs n_I when $r = 1$ and (b) μ_I/μ_S vs r when $n_I = 0.3$. For both the cases $n_S = 0.8$, $K_f = 0.95$ and $L_f = 0.095$ are the fixed parametrs and the optical quantum efficiencies ($\eta_{I,S}$) are considered to be 1. Black lines stand for the maximal of squeezing, and white lines indecate the boundary of SQL.

Funding. HORIZON EUROPE Marie Sklodowska-Curie Actions (101065991).

Acknowledgments. SA would like to thank Kishore Thapliyal for his fruitful suggestions. The work has been supported by the European Commission, MSCA GA no 101065991 (SingletSQL).

Disclosures. The author has no conflicts to disclose.

Data availability. No data were generated or analyzed in the presented research.

References

1. A. Einstein, B. Podolsky, and N. Rosen, "Can quantum-mechanical description of physical reality be considered complete?" Phys. Rev. **47**(10), 777–780 (1935).
2. J. S. Bell, "On the Einstein Podolsky Rosen paradox," Phys. Physique Fizika **1**(3), 195–200 (1964).
3. D. Stucki, M. Legré, F. Buntschu, *et al.*, "Long-term performance of the SwissQuantum quantum key distribution network in a field environment," New J. Phys. **13**(12), 123001 (2011).
4. A. Barenco, D. Deutsch, A. Ekert, *et al.*, "Conditional quantum dynamics and logic gates," Phys. Rev. Lett. **74**(20), 4083–4086 (1995).
5. S. L. Braunstein and H. J. Kimble, "Teleportation of continuous quantum variables," Phys. Rev. Lett. **80**(4), 869–872 (1998).
6. S. Agasti, A. Shukla, and M. Nesladek, "Negative radiation pressure scheme for simultaneous suppression of arduous back-action evasion and shot noise in gravitational wave detectors," Classical Quantum Gravity **42**(6), 065021 (2025).

Optics EXPRESS

7. M. B. Plenio and S. F. Huelga, "Entangled light from white noise," Phys. Rev. Lett. **88**(19), 197901 (2002).
8. H. Jeong, J. Lee, and M. S. Kim, "Dynamics of nonlocality for a two-mode squeezed state in a thermal environment," Phys. Rev. A **61**(5), 052101 (2000).
9. A. Gilchrist, P. Deuar, and M. D. Reid, "Contradiction of quantum mechanics with local hidden variables for quadrature phase amplitude measurements," Phys. Rev. Lett. **80**(15), 3169–3172 (1998).
10. W. J. Munro, "Optimal states for bell-inequality violations using quadrature-phase homodyne measurements," Phys. Rev. A **59**(6), 4197–4201 (1999).
11. J. F. Clauser, M. A. Horne, A. Shimony, *et al.*, "Proposed experiment to test local hidden-variable theories," Phys. Rev. Lett. **23**(15), 880–884 (1969).
12. J. F. Clauser and M. A. Horne, "Experimental consequences of objective local theories," Phys. Rev. D **10**(2), 526–535 (1974).
13. M. Takeoka and M. Sasaki, "Conditional generation of an arbitrary superposition of coherent states," Phys. Rev. A **75**(6), 064302 (2007).
14. O. Haderka, J. Peřina, M. Hamar, *et al.*, "Direct measurement and reconstruction of nonclassical features of twin beams generated in spontaneous parametric down-conversion," Phys. Rev. A **71**(3), 033815 (2005).
15. S. Agasti, "Numerical simulation of kerr nonlinear systems; analyzing non-classical dynamics," J. Phys. Commun. **3**(10), 105004 (2019).
16. S. Agasti, "Simulation of kerr nonlinearity: revealing initial state dependency," Phys. Scr. **98**(11), 115103 (2023).
17. M. Asjad, P. Tombesi, and D. Vitali, "Feedback control of two-mode output entanglement and steering in cavity optomechanics," Phys. Rev. A **94**(5), 052312 (2016).
18. S. Zippilli, G. D. Giuseppe, and D. Vitali, "Entanglement and squeezing of continuous-wave stationary light," New J. Phys. **17**(4), 043025 (2015).
19. C. Genes, A. Mari, P. Tombesi, *et al.*, "Robust entanglement of a micromechanical resonator with output optical fields," Phys. Rev. A **78**(3), 032316 (2008).
20. L.-M. Duan, G. Giedke, J. I. Cirac, *et al.*, "Inseparability criterion for continuous variable systems," Phys. Rev. Lett. **84**(12), 2722–2725 (2000).
21. S. Barzanjeh, S. Guha, C. Weedbrook, *et al.*, "Microwave quantum illumination," Phys. Rev. Lett. **114**(8), 080503 (2015).
22. J. Meinel, V. Vorobyov, B. Yavkin, *et al.*, "Heterodyne sensing of microwaves with a quantum sensor," Nat. Commun. **12**(1), 2737 (2021).
23. J. Peřina, V. Michálek, R. Machulka, *et al.*, "Two-beam light with simultaneous anticorrelations in photon-number fluctuations and sub-poissonian statistics," Phys. Rev. A **104**(1), 013712 (2021).
24. M. Tillmann, S.-H. Tan, S. E. Stoeckl, *et al.*, "Generalized multiphoton quantum interference," Phys. Rev. X **5**(4), 041015 (2015).
25. C. Fabre and N. Treps, "Modes and states in quantum optics," Rev. Mod. Phys. **92**(3), 035005 (2020).
26. T. Hiroshima, "Decoherence and entanglement in two-mode squeezed vacuum states," Phys. Rev. A **63**(2), 022305 (2001).
27. J. S. Prauzner-Bechcicki, "Two-mode squeezed vacuum state coupled to the common thermal reservoir," J. Phys. A: Math. Gen. **37**(15), L173–L181 (2004).
28. M. S. Kim, J. Lee, and W. J. Munro, "Experimentally realizable characterizations of continuous-variable gaussian states," Phys. Rev. A **66**(3), 030301 (2002).
29. J. H. Eberly and K. Wódkiewicz, "The time-dependent physical spectrum of light*," J. Opt. Soc. Am. **67**(9), 1252–1261 (1977).
30. R. Simon, "Peres-horodecki separability criterion for continuous variable systems," Phys. Rev. Lett. **84**(12), 2726–2729 (2000).
31. S. Agasti, "Thermalization dynamics of entanglement and non-locality of filtered two-mode squeezed states," Opt. Express **33**(3), 4420–4436 (2025).
32. M. G. A. Paris, F. Illuminati, A. Serafini, *et al.*, "Purity of gaussian states: Measurement schemes and time evolution in noisy channels," Phys. Rev. A **68**(1), 012314 (2003).
33. K. Banaszek and K. Wódkiewicz, "Nonlocality of the einstein-podolsky-rosen state in the wigner representation," Phys. Rev. A **58**(6), 4345–4347 (1998).
34. K. Banaszek and K. Wódkiewicz, "Testing quantum nonlocality in phase space," Phys. Rev. Lett. **82**(10), 2009–2013 (1999).
35. D. Girolami, "Quantum correlations in information theory," Ph.D. thesis, Nottingham U. (2013).